Supporting information

Manuscript titled: Self-assembled 2D soft supramolecular networks characterized by STM/STS in air and under vacuum

Authors: Borislav Naydenov, Samuel Torsney, Alejandro Santana Bonilla, Mohamed El Garah, Artur Ciesielski, Andrea Gualandi, Luca Mengozzi, Pier Giorgio Cozzi, Rafael Gutierrez, Paolo Samorì, Gianaurelio Cuniberti, and John J. Boland

Number of pages: 12
Number of figures: 12
Number of tables: 3

A. UHV-STM topography – experiment

In figure S1 are presented simultaneously taken images of a M2-island. The lack of image changes can be observed in all typographs in the -1.0V to +1.2V sample bias range.

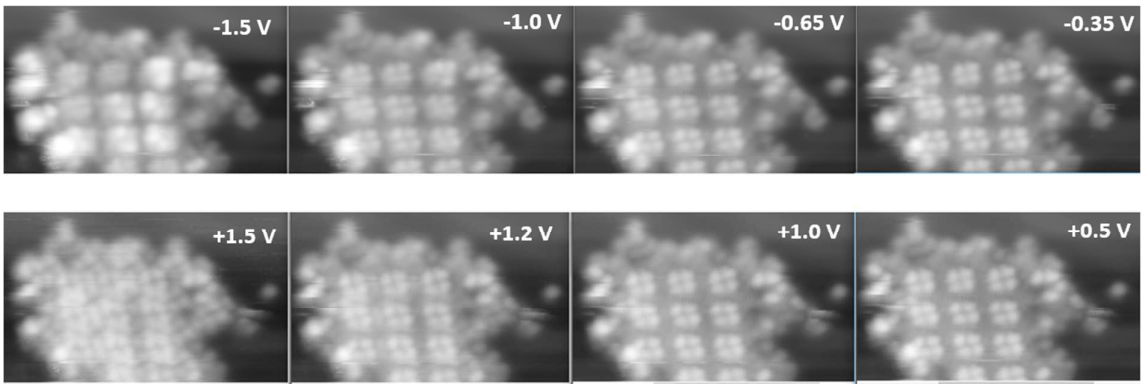

Fig. S1. UHV-STM topographic images of M2 molecules self-assembled in an island on Au(111) surface, recorded simultaneously. The tunneling current of 20pA is identical for all images and the corresponding sample biases are denoted on the top-right corner of each image.

In figure S2 STM images in air and in vacuum are compared to demonstrate the different appearances under the two environments at similar bias conditions.

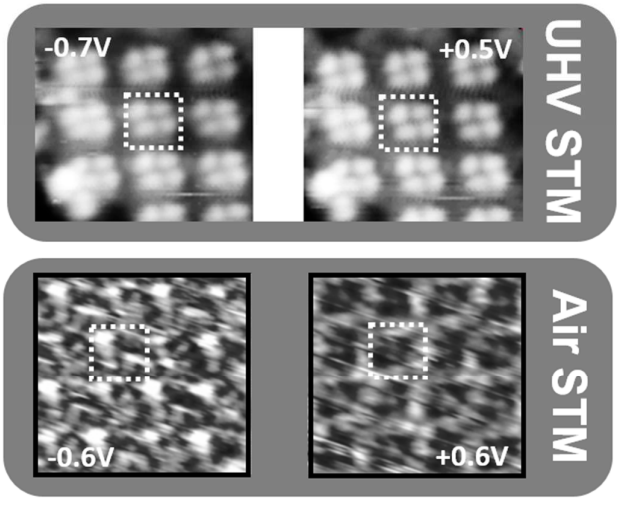

Fig. S2. STM topographic images of self-assembled M2 molecules on Au(111) surface in vacuum and in air..

B. Adsorption geometry – theory

In Figure S3 are presented the two planar configurations (C1 and C2) of the optimized unit cells for M1 and M2. The M1C1 and M2C2 being the lowest in total energy configurations.

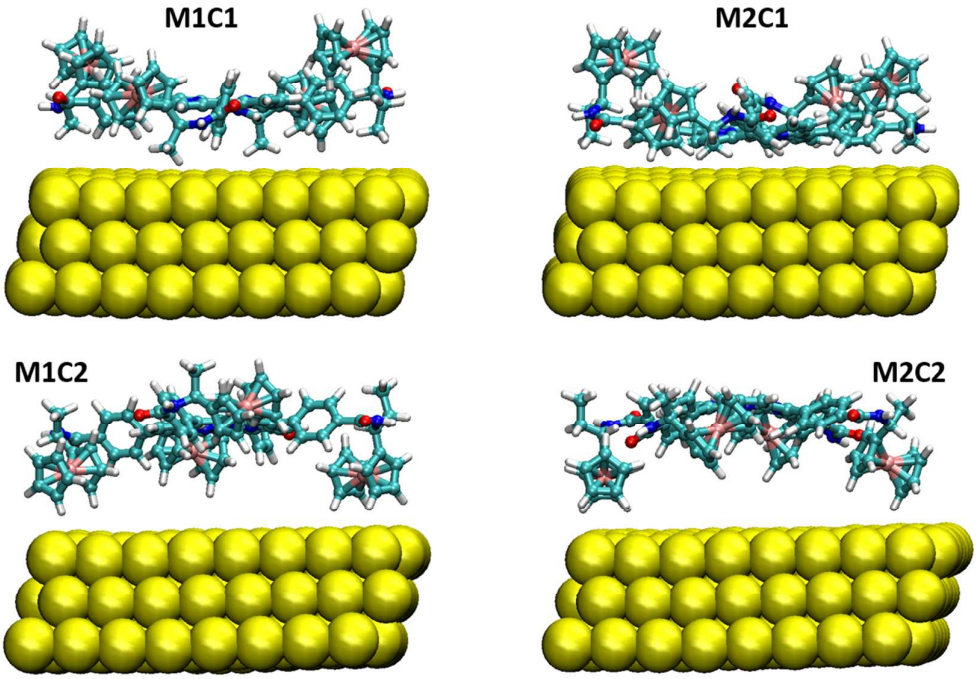

Fig. S3. Side views of the two planar configurations (C1 and C2) of the optimized unit cells for M1 and M2.

C. Electronic properties - theory

Au(111) slab optimization: In order to simulate the surface, the slab technique has been used. Thus, a three atomic layer of the Au(111) surface has been formed. In the perpendicular direction to the Au(111) surface a vacuum separation of 30 Å has been added so as to avoid spurious interactions between the neighboring slabs. At this stage, both the unit cell and the geometry have been optimized for the initial slab. In this case the rev-PBE exchange-correlation implementation has been used [1]. The structure has been relaxed until the atomic displacements were lower than 9×10^{-4} Bohr and the forces lower than 4.5×10^{-4} Hartree/Bohr. The relaxed lattice vector (2.88 Å) of the unit cell for the Au(111) slab is in good agreement

with the ones theoretically and experimentally obtained [2]. Subsequently, we have calculated the work function of our metallic slab using the usual definition of: $\Phi = \varphi_0 - E_F$, where φ_0 is the electrostatic potential in the vacuum region and E_F is the Fermi level of the metal [2]. In Table I, we collect all the values of the work functions for the different XC implementations. Interestingly, the PBE0-TC-LR implementation delivers a work function value that is in good agreement with the reported results from both computational and experimental studies (5.2-5.35 eV) [2]. This indicates that the PBE0-TC-LR implementation is a suitable functional that can qualitatively describe both subsystems, namely, the organometallic molecular and the metallic surface providing a qualitatively accurate physical picture of the system.

TABLE S1. Theoretical values calculated for the three-layer Au(111) slab for different XC implementations.

Exchange-Correlation (XC)	**E Fermi (eV)**	**V(Z) (eV)**	**Φ(eV)**
PBEsol	-3.48	1.83	5.31
TPSS	-3.37	1.95	5.32
PBE0-TC-LR	-4.05	1.55	5.60

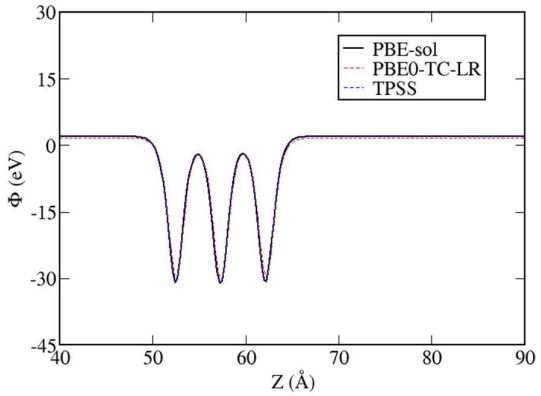

Fig. S4. Computed plane-averaged electrostatic potential for the Au(111) slab. Three different XC functionals have been used. The φ_0 parameter has been obtained from this procedure allowing us to calculate the work function in each case ($\Phi = \varphi_0 - E_F$).

XC benchmarking of the isolated and periodic monolayer for M1 and M2: The electronic structure of the isolated molecule is presented in Fig. S5 and S6, where the organization of the energy levels and the first 10 states are displayed. As it is mentioned in the main text, the XC implementation used in order to investigate the system plays a fundamental role especially in the case of the organometallic complexes. In this sense some experimental and theoretical work has been carried out showing that further functionalization of the

ferrocene moieties leads to a splitting of the ideal *d*-orbital ordering [2,3]. Likewise, the separation amid the energy levels (≈ 290 meV in both cases) is quite small leading to a possible hybridization between adjacent energy levels. This is important in the formation of the electronic structure for the supramolecular networks. Once the 2D network is formed narrow bands will be formed by hybridization of the molecular states leading to possible formation of linear combinations of the different contributing ferrocene states at different geometrical positions within the molecular complex.

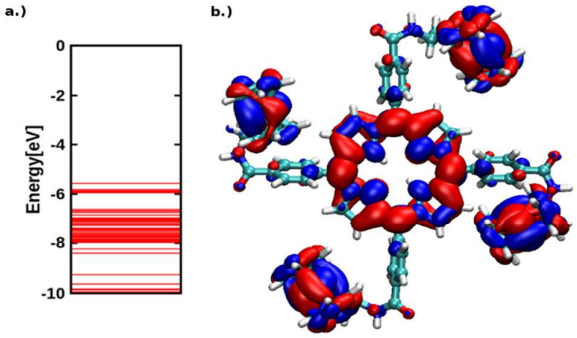

Fig. S5. (a) Orbital energy levels and (b) Ten first frontier molecular orbitals for the M1 complex.

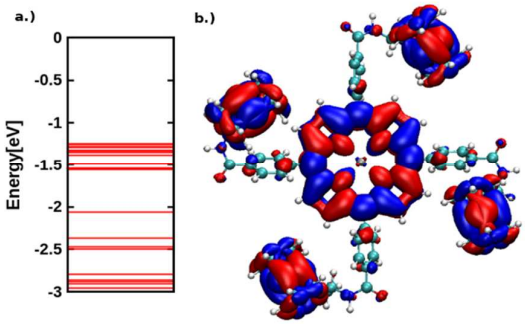

Fig. S6. (a) Orbital energy levels and (b) Ten first frontier molecular orbitals for the M2 complex.

In this case, we find an underestimation in the energy gap in the TPSS and PBEsol XC implementations. The transport energy gap is estimated via the formula E_transp=IP-EA, see the main text. Hence, the underestimation of the molecular gap is due to the self-interaction, which is partially corrected in the short-range PBE0 implementation of the PBE0-TC-LR exchange correlation. Hence, based on the results obtained from this benchmark procedure, we observe that the PBE0-TC-LR exchange-correlation implementation offers a much better description of the electronic structure for both gas and periodic monolayer while preserving a reasonable computational cost.

TABLE S2. Theoretical values calculated for the M1 complex for different XC implementations

Exchange-Correlation	**IP(eV)**	**EA(eV)**	**IP-EA(eV)**
PBESOL	5.35	1.70	3.65
TPSS	4.91	1.46	3.45
PBE0-TC-LR	5.91	2.01	3.9

TABLE S3. Theoretical values calculated for the M2 complex for different XC implementations

Exchange-Correlation	**IP (eV)**	**EA(eV)**	**IP-EA (eV)**
PBESOL	4.98	2.05	2.93
TPSS	4.95	1.60	3.35
PBE0-TC-LR	5.88	2.12	3.76

ELF plots: The Electron Localization Function (ELF) calculated for the molecular complexes showing the kind of bond presented by the molecule. Thus, the non-covalent interactions such as vdW and Coulomb interactions are the more important contributions in our total system since the ELF numbers range from 0.4 to 0.6 in the color scale shown in Fig. S7 and S8.

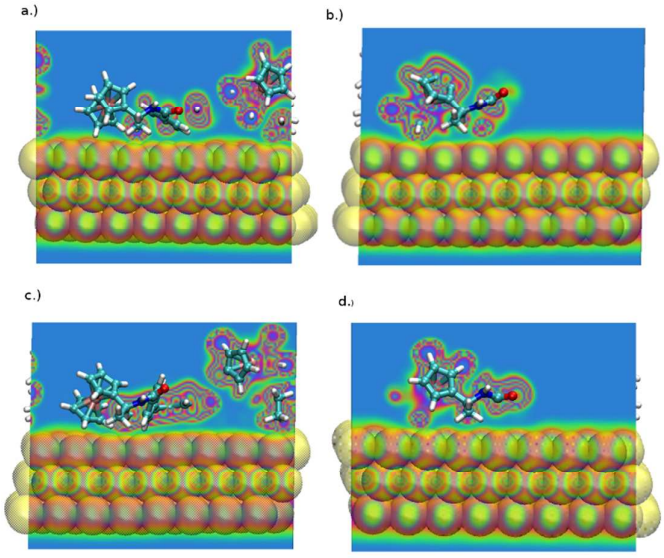

Fig. S7. Electron Localization Function (ELF) for the M1 molecular complex. The color scale indicates the kind of bond observed and spatially resolved leading to conclude that this molecule is physisorbed over the Au(111) surface.

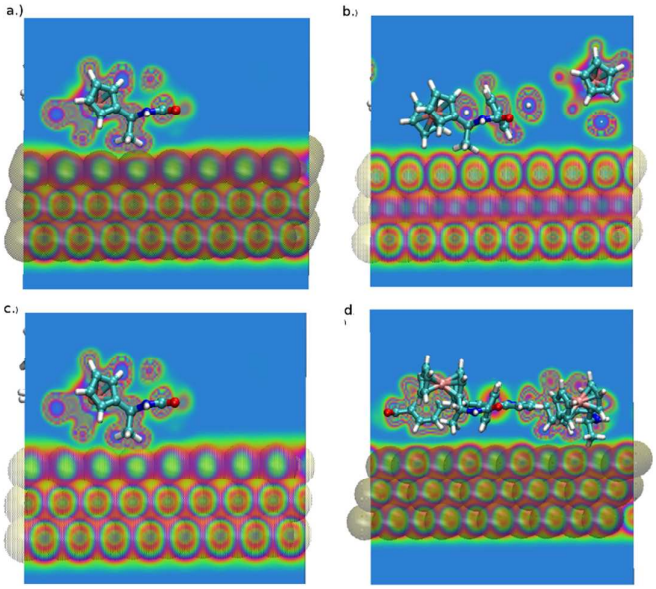

Fig. S8. Electron Localization Function (ELF) for the M2 molecular complex. The color scale indicates the kind of bond observed and spatially resolved leading to conclude that this molecule

The electronic structure of the total system is investigated with a special emphasis on the alignment between the discrete molecular energy levels supplied by the molecular complexes with the continuum states of the metal surface. This is important since a possible hybridization of the localized *d*-molecular orbitals provided by the ferrocene moiety and the surface *d*-states in Au(111) can lead to charge transfer (CT). CT can take place through direct overlap of the molecular orbitals and/or through the alignment of the Fermi levels of both systems [4]. Determining which factor dominates is challenging and requires a detailed analysis of the metal-molecule interface. In our specific case, the correct description of the molecule´s energy levels position strongly depends on the choice of an appropriate exchange-correlation (XC) parametrization, especially for the estimation of the correct molecular energy gap. Thus, e.g. in the case of organometallic complexes, the usage of hybrid functionals is preferred over semi-local generalized gradient approximations (GGA) [5]. Nonetheless, it is precisely the introduction of a certain percentage of the exact exchange (HFX) term which deprecates the description of the metallic nature of the slab [6, 7]. We therefore use a new implementation where the Coulomb interaction is split into short-range (SR) and long-range (LR) contributions, which leads to a much better description of solids and gives us the opportunity to study the accuracy of this implementation in order to understand the challenging organometallic-surface interaction [8].

D. Synthesis of M1 and M2

D.1 General Methods

^{1}H NMR spectra were recorded on Varian Mercury 400 and Inova 600 spectrometers. Chemical shifts are reported in ppm from TMS with the solvent resonance as the internal standard (deuterochloroform: δ = 7.27 ppm). Data are reported as follows: chemical shift, multiplicity (s = singlet, d = duplet, t = triplet, q = quartet, dd = double duplet, dt = double triplet, pd = pseudo duplet, pt = pseudo triplet, m = multiplet), coupling constants (Hz). ^{13}C NMR spectra were recorded on Varian MR400 spectrometer. Chemical shifts are reported in ppm from TMS with the solvent as the internal standard (deuterochloroform: δ= 77.0). LC-electrospray ionization mass spectra (ESI-MS) were obtained with Agilent Technologies MSD1100 single-quadrupole mass spectrometer. They are reported as: *m/z* (rel. intense). Electrospray Ion Trap Mass Spectrometry were obtained with Agilent Technologies LC/MSD 1100 ion trap mass spectrometer injecting a solution in chloroform/methanol of the pure compound. Chromatographic purification was done with 240-400 mesh silica gel. Purification on preparative thin layer chromatography was done on Merck TLC silica gel 60 F_{254}.

D.2 Materials and synthesis

If not otherwise stated, all reactions were carried under anhydrous conditions using standard Schlenk apparatus. Anhydrous solvents were supplied by Aldrich in Sureseal® bottles and were used as received avoiding further purification.

Reagents were purchased from Aldrich or TCI and used without further purification unless otherwise stated.

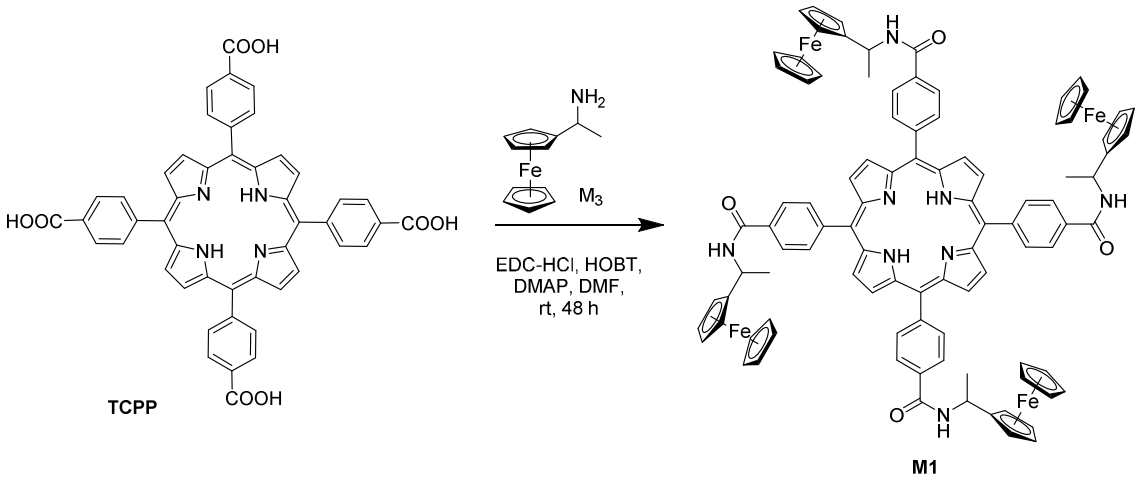

*Fig. S9. Synthesis of **M1***

M1: In a 10 mL round bottomed flask under nitrogen atmosphere, TCPP (100 mg, 0.12 mmol) was dissolved in DMF (4 mL). *N*-(3-Dimethylaminopropyl)-*N*′-ethylcarbodiimide (EDC) hydrochloride (144 mg, 0.76 mmol) and hydroxybenzonitrile (HOBT) (102 mg, 0.76 mmol) were added. The solution was shielded by light and stirred for 1 h. Then 1-ferrocenyl-1-ethyl amine[1] **M3** (130 mg, 0.56 mmol) and DMAP (70 mg, 0.56 mmol) were added. After 48 hours the reaction was diluted with DCM (30 mL) and washed 5 times with water (10 mL). The organic phase was concentrated and purified by column chromatography (49:49:2 ethyl acetate:cyclohexane:DCM) to afford pure **M1** (73 % yield, 142 mg, 0.087 mmol) as a dark purple solid (m.p. not observed up to 320°C).

^{1}H NMR (400 MHz, $CDCl_3$) δ = 8.83 (s, 8H), 8.30 (d, J = 7.6 Hz, 8H), 8.19 (d, J = 7.7 Hz, 8H), 6.68 (d, J = 7.6 Hz, 4H), 5.28 (m, 4H), 4.44 (s, 4H), 4.38 (s, 4H), 4.33 (s, 20H), 4.29 (s, 4H), 4.27 (s, 4H), 1.74 (d, J = 6.5 Hz, 12H), -2.81 (s, 2H); ^{13}CNMR (100 MHz, $CDCl_3$, 25°C): δ = 166.1 (4C), 145.1 (4C), 134.6 (8C), 134.3 (4C), 131.2 (bs, 8C), 125.3 (8C), 119.3 (4C), 91.4 (4C), 68.7 (20C), 68.4 (4C), 68.0 (4C), 67.7 (4C), 65.9 (4C), 44.5 (4C), 20.8 (4C), (we were unable to detect one signal relative to the 8 carbons of the porphyrin core).

Mass calculated for $C_{96}H_{82}Fe_4N_8O_4$: 1634.4. ESI-MS: m/z = 1635.4 $[M+H]^+$.

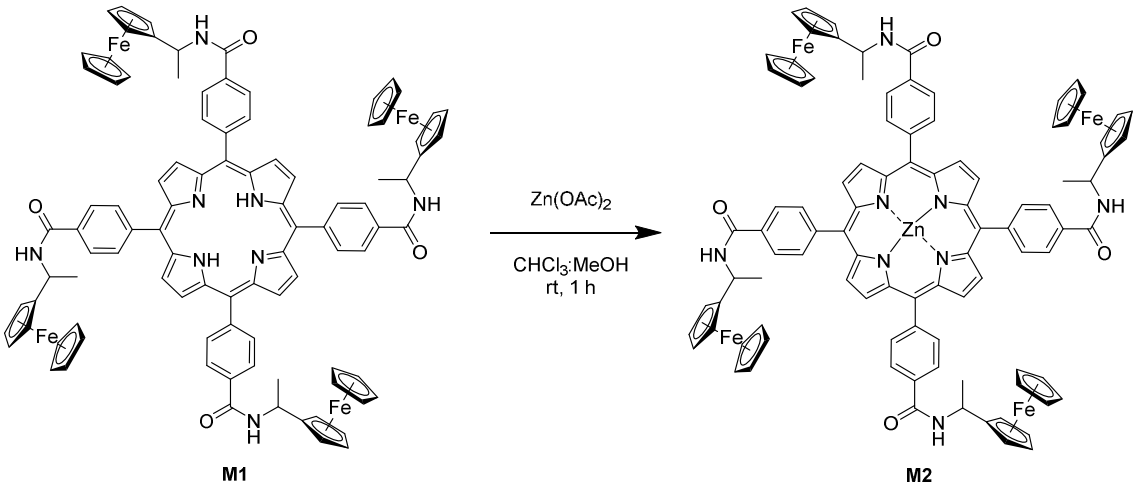

*Fig. S10. Synthesis of **M1***

M2: In a 10 mL round bottomed flask under nitrogen atmosphere, **M1** (30 mg, 0.018 mmol) was dissolved in $CHCl_3$ (1.3 mL). Then a solution of $Zn(OAc)_2 \cdot 2H_2O$ (4.0 mg 0.018 mmol) in methanol (400 μL) was added dropwise by syringe and the resulting solution was stirred for 3 h until complete conversion was observed by TLC analysis. The reaction mixture was diluted with DCM (5 mL) washed with water (5 mL). The organic phase was separated and dried under reduced pressure to afford pure **M2** (94% yield, 29 mg, 0.017 mmol) as a dark purple solid (m.p. not observed up to 320°C).

^{1}H NMR (400 MHz, $CDCl_3$) δ = 8.90 (s, 8H), 8.20-8.30 (bs, 8H), 7.90-8.05 (bs, 8H), 6.53-6.66 (bs, 4H), 4.88-5.05 (bs, 4H), 4.32-4.42 (bs, 4H), 4.10-4.41 (bs, 32H), 1.56-1.68 (bs, 12H); ^{13}CNMR (100 MHz, $CDCl_3$, 25°C): δ = 165.8 (4C), 149.8 (8C), 146.2 (4C), 134.6 (8C), 133.4 (4C), 132.0 (8C), 124.9 (8C), 120.0 (4C), 91.5 (4C), 68.7 (20C), 68.4 (4C), 68.1 (4C), 67.8 (4C), 66.0 (4C), 44.2 (4C), 20.6 (4C).

Exact mass calculated for $C_{96}H_{80}Fe_4N_8O_4Zn$ 1696.3. ESI-MS: *m/z* = 1697.6 $[M+H]^+$; 1719.5 $[M+Na]^+$.

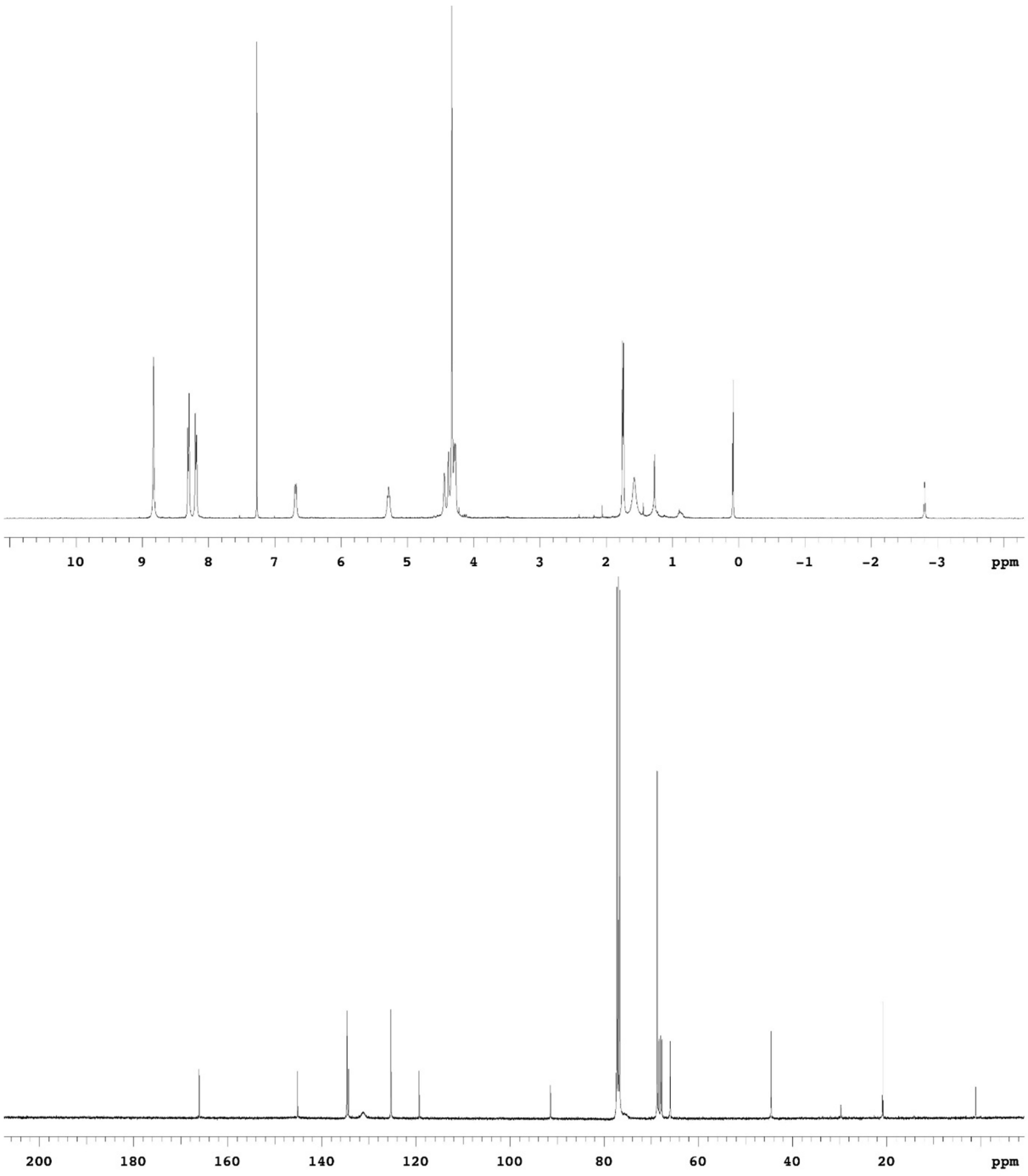

*Fig. S11. NMR spectra of **M1***

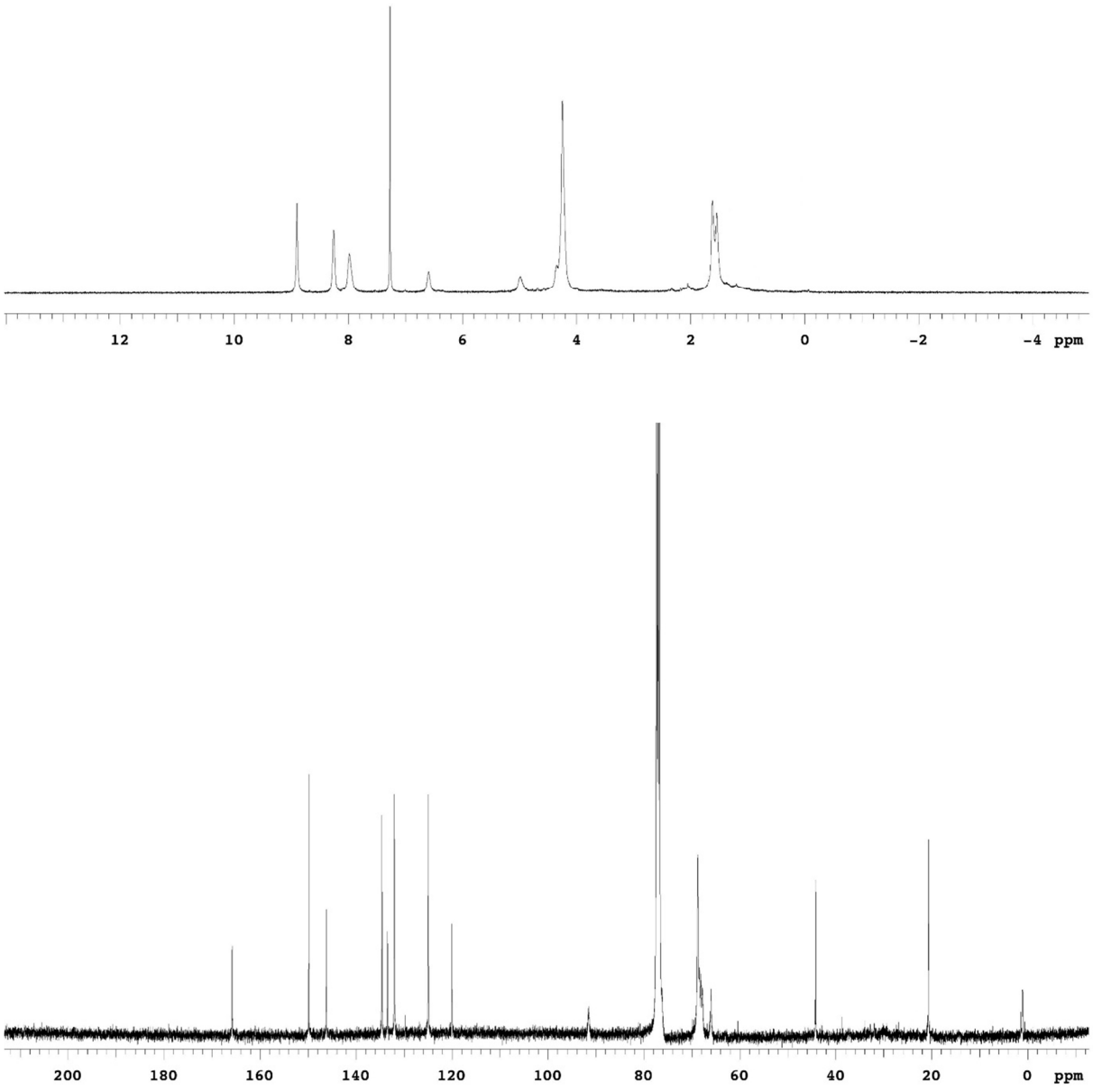

*Fig. S12. NMR spectra of **M2***

[1] For the synthesis of 1-ferrocenyl-1-ethyl amine see: Iurlo M.; Mengozzi L.; Rapino S.; Marcaccio M.; Perone R.C.; Masiero S.; Cozzi P.; Paolucci F. *Organometallics*, **2014**, *33*, 4986−4993.

References:

[1] Z.Yhang and W. Yang, Phys. Rev. Lett. 80, 890 (1998).

[2] Paul C. Rusu and Geert Brocks, J. Phys. Chem. B, 2006, 110 (45), 22628–22634

[3] Lijuan Zhang, Dongdong Qi, Yuexing Zhang, Yongzhong Bian, Jianzhuang Jiang, Journal of Molecular Graphics and modelling 29 (2011) 717-725

[4] Koch, N., N. Ueno, and A.T.S. Wee, Molecule-Metal Interface, 2013: p. Xi-Xii.

[5] Zhang, W.J., D.G. Truhlar, and M.S. Tang, Journal of Chemical Theory and Computation, 2013. **9**(9): p. 3965-3977.

[6] Kurth, S., J.P. Perdew, and P. Blaha, International Journal of Quantum Chemistry, 1999. **75**(4-5): p. 889-909.

[7] Paier, J., et al.,Journal of Chemical Physics, 2006. **125**(24).

[8] Heyd, J. and G.E. Scuseria, Journal of Chemical Physics, 2004. **120**(16): p. 7274-7280.